Stoch Environ Res Risk Assess
DOI 10.1007/s00477-008-0272-0

ORIGINAL PAPER

Nonlinear extensions of a fractal–multifractal approach for environmental modeling

Andrea Cortis · Carlos E. Puente · Bellie Sivakumar

Abstract We present the extension of a deterministic fractal geometric procedure aimed at representing the complexity of patterns encountered in environmental applications. The procedure, which is based on transformations of multifractal distributions via fractal functions, is extended through the introduction of nonlinear perturbations in the generating iterated linear maps. We demonstrate, by means of various simulations based on changes in parameters, that the nonlinear perturbations generate yet a richer collection of interesting patterns, as reflected by their overall shapes and their statistical and multifractal properties. It is shown that the nonlinear extensions yield structures that closely resemble complex hydrologic spatio-temporal datasets, such as rainfall and runoff time series, and width-functions of river networks. The implications of this nonlinear approach for environmental modeling and prediction are discussed.

Keywords Modeling · Fractals · Multifractals · Iterated maps

A. Cortis (✉)
Earth Sciences Division,
Lawrence Berkeley National Laboratory,
Berkeley, CA 94720, USA
e-mail: acortis@lbl.gov

C. E. Puente · B. Sivakumar
Department of Land, Air and Water Resources,
University of California, Davis, CA 95616, USA
e-mail: cepuente@ucdavis.edu

B. Sivakumar
e-mail: sbellie@ucdavis.edu

1 Introduction

Mathematical methods based on stochastic approaches (e.g., Box et al. 1994; Yaglom 1987) and on fractal geometry and chaos theory (e.g., Mandelbrot 1983; Lorenz 1963) have now long been used as a suitable language for the description of the complexities so often encountered in natural phenomena. These notions, however, are oftentimes insufficient to study, on an individual basis, the incredible variety of patterns observed in nature. Given that natural sets (i.e., time series, spatial patterns, space–time sets) are typically erratic, noisy, intermittent, nonsmooth, or in short "random," it has become natural to model them using stochastic (fractal) theories. Such modeling has resulted in a variety of procedures that, while yielding realizations that preserve some of the relevant statistical and fractal attributes of the records (e.g., autocorrelation function, power spectrum, moments, multifractal spectrum, etc.), are typically unable to capture all the specific details and textures present in individual sets.

As stochastic approaches, by definition, can only generate plausible realizations preserving only some features of the data, and as studies of nonlinear dynamics have revealed that details indeed matter (e.g., in climate studies; Lorenz 1963), the following questions have become inevitable: (a) Is it possible to devise a modeling approach that faithfully models individual patterns capturing not only the overall trends and statistical features of the records but also their inherent details? (b) Can such an approach be defined without resorting to the concept of randomness, implying an inherent hidden order in complexity as found in deterministic chaos? (c) Can such an approach, by the capturing of details, be helpful in studying the underlying dynamics of such sets?

It is now well known that a large class of deterministic fractal sets can be generated via iterations of simple linear

maps (e.g., Barnsley 1988). Puente (1992) described how fractal interpolation functions (defined as attractors of simple linear maps) transform multifractal distributions into deterministic derived measures that mimic the complexity of patterns found in nature. The present work reviews and extends this deterministic fractal geometric approach. The extensions entail adding bounded nonlinear perturbations to the above-mentioned iterated linear maps to produce yet more exotic attractors and subsequent deterministic derived measures. As shall be demonstrated herein, the addition of such perturbations uncovers a vast class of relevant patterns over one dimension that closely resemble those found in a variety of environmental fields. These patterns turn out to be parsimoniously encoded via few geometric parameters (i.e., the quantities that define the involved maps, their perturbations and how iterations are performed) and, given the simplicity of the algorithm that generates them, are therefore amenable for applications.

The organization of this paper is as follows. Given first is a review of the original mathematical construction and a description of the nonlinear extensions. This is followed by a variety of examples based on a host of evolutions, obtained varying few parameters, that include statistical and multifractal analysis of the patterns. Finally, the relevance of this enhanced approach to environmental modeling is discussed and directions for future work are sketched.

2 The fractal–multifractal approach

The graph G of a fractal interpolating function, from x to y and passing by $N+1$ points on the plane $\{(x_n, y_n);\ x_0 < \cdots < x_N\}$, is defined by iterating N linear maps, $n = 1,\ldots, N$ (e.g., Barnsley 1986):

$$w_n\begin{pmatrix} x \\ y \end{pmatrix} = \begin{pmatrix} a_n & 0 \\ c_n & d_n \end{pmatrix}\begin{pmatrix} x \\ y \end{pmatrix} + \begin{pmatrix} e_n \\ f_n \end{pmatrix}, \tag{1}$$

such that $|d_n| < 1$ and

$$w_n\begin{pmatrix} x_0 \\ y_0 \end{pmatrix} = \begin{pmatrix} x_{n-1} \\ y_{n-1} \end{pmatrix}, \quad w_n\begin{pmatrix} x_N \\ y_N \end{pmatrix} = \begin{pmatrix} x_n \\ y_n \end{pmatrix}. \tag{2}$$

The two initial conditions in Eq. 2 lead to simultaneous sets of linear equations that allow calculation of the parameters a_n, c_n, e_n, and f_n in terms of the interpolating points and the vertical scalings d_n, as follows:

$$a_n = \frac{x_n - x_{n-1}}{x_N - x_0} \tag{3}$$

$$e_n = x_{n-1} - x_0 \cdot a_n \tag{4}$$

$$c_n = \frac{y_n - y_{n-1} - d_n(y_N - y_0)}{x_N - x_0} \tag{5}$$

$$f_n = y_{n-1} - c_n \cdot x_0 - d_n \cdot y_0 \tag{6}$$

Equation 2 ensures that G (the attractor obtained by arbitrarily iterating the linear maps) exists and that it is a continuous function that contains the initial interpolating points (e.g., Barnsley 1986; Puente 1992). As the same attractor G is found irrespective of how the iterations are performed (i.e., with fair or biased proportions on the N maps w_n), such a unique set is fully deterministic. Depending on the parameters, G turns out to have a fractal dimension $D \in [1, 2)$ (Barnsley 1988).

As the process of iterations is carried out, effectively sampling G point by point, not only is the attractor being computed but also a unique invariant measure over G is induced, which reflects how the attractor is being filled up. The existence of such a measure allows computing unique (and once again fully deterministic) projections over the coordinates x and y (say dx and dy) that turn out to have interesting shapes, as found in a variety of environmental applications and beyond (e.g., Puente 1996, 2004).

Figure 1 shows an example of these ideas for a fractal interpolating function (having a fractal dimension $D = 1.485$) that passes by the three points $\{(0, 0), (1/2, -0.35), (1, -0.2)\}$ when the vertical scalings of the $N = 2$ mappings w_n are $d_1 = -0.8$ and $d_2 = -0.6$. In addition to the graph of the attractor G, clearly a continuous function from x to y, the figure also includes the implied projections dx and dy of the unique measure found over G when the corresponding mappings w_1 and w_2 are iterated (2^{19} times) according to a 30–70% proportion, using independent pseudo-random numbers, starting the process from the mid-point $(1/2, -0.35)$.

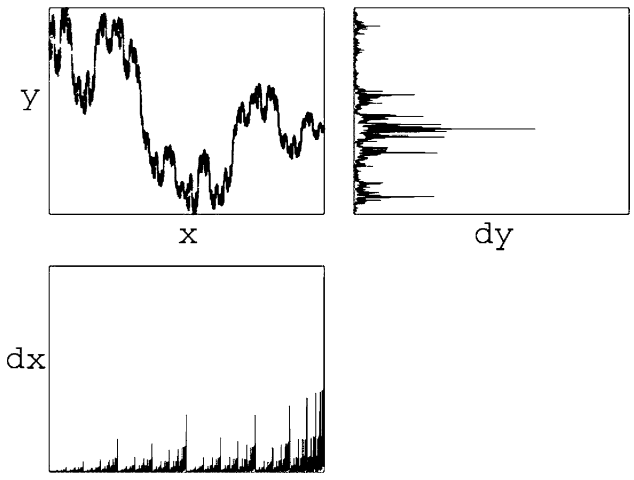

Fig. 1 From a multifractal measure dx to a derived measure dy via a continuous fractal interpolating function from x to y found via the iteration of linear maps. Interpolating points: $\{(0, 0), (1/2, -0.35), (1, -0.2)\}$, vertical scalings: $d_1 = -0.8$, $d_2 = -0.6$, parent multifractal parameter: $p = 0.3$. (Measures dx and dy are normalized so that they add up to one and they are computed over 4,096 bins)

As the x coordinate of the linear maps does not depend on y (as implied by the 0 value in the first component of Eq. 1), the measure dx turns out to be a deterministic binomial multifractal with parameter $p = 0.3$, as defined via a simple multiplicative cascade (Mandelbrot 1989). The measure dy, on the other hand, being related to dx via the fractal interpolating function whose graph is G, turns out to be the derived measure of dx via such a function and is, hence, computed numerically adding all measure values over x that correspond to a given value of y (e.g., Puente 1994, 1996). Notice that this projection may be computed at a general angle θ, other than at 0° as shown in Fig. 1 over the y axis.

As may be seen, the procedure leads to complex and "random-looking" measures dy (i.e., the projection over the y axis) that resemble environmental time series, such as rainfall as a function of time (Puente and Obregón 1996). As multifractal measures are relevant in the study of turbulence over one dimension (e.g., Meneveau and Sreenivasan 1987), the projection sets, dy, obtained integrating a turbulence-related dx via a fractal interpolating function, may be assigned an interpretation as "reflections" or more precisely "transformations" of turbulence (Puente and Sivakumar 2007).

3 Nonlinear extensions of the fractal–multifractal approach

A suitable way to extend the fractal–multifractal approach is to add a bounded nonlinear perturbation $g(y)$ on the y component of the linear maps previously introduced, as follows:

$$w_n\begin{pmatrix} x \\ y \end{pmatrix} = \begin{pmatrix} a_n & 0 \\ c_n & d_n \end{pmatrix}\begin{pmatrix} x \\ y + g(y) \end{pmatrix} + \begin{pmatrix} e_n \\ f_n \end{pmatrix}. \tag{7}$$

This yields, using the same set of initial conditions as before (Eq. 2), the following modified parameters c_n and f_n that now depend also on the specific choice of the nonlinear function g:

$$c_n = \frac{y_n - y_{n-1} - d_n(y_N + g(y_N) - y_0 - g(y_0))}{x_N - x_0} \tag{8}$$

$$f_n = y_{n-1} - c_n \cdot x_0 - d_n \cdot (y_0 + g(y_0)) \tag{9}$$

Figure 2 shows an example of what is obtained when adding a cosine perturbation of the form $g(y) = A \cdot \cos(\omega \cdot y)$, for an amplitude $A = 0.5$ and a frequency $\omega = 1$, while using the same set of parameters employed for the linear case in Fig. 1. As may be noticed, this nonlinear case results in an attractor that is now a sparse collection of points, unlike the linear case in which successive points do agglomerate into a single continuous function. Such an attractor set turns out to be a

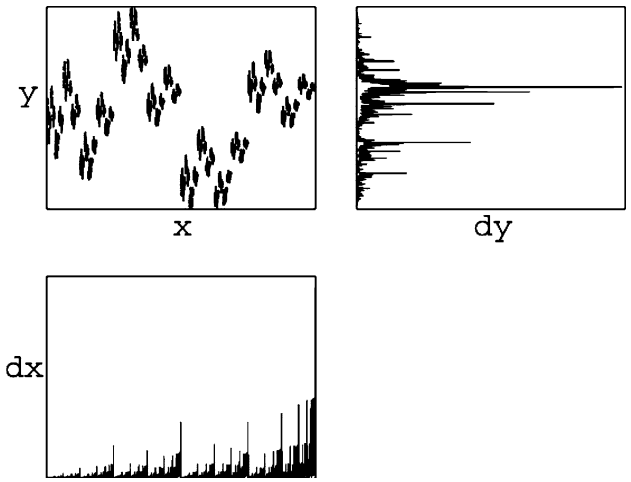

Fig. 2 From a multifractal measure dx to a derived measure dy via a fractal attractor from x to y found via the iteration of nonlinear maps. Interpolating points: {(0, 0), (1/2, −0.35), (1, −0.2)}, vertical scalings: $d_1 = -0.8$, $d_2 = -0.6$, parent multifractal parameter: $p = 0.3$, nonlinear perturbation: $g(y) = A \cdot \cos(\omega \cdot y)$, $A = 0.5$, $\omega = 1$. (Measures dx and dy are normalized so that they add up to one and they are computed over 4,096 bins)

mathematical fractal that repeats itself under increasing magnification and that has a fractal dimension similar to that of the interpolating function shown in Fig. 1 (i.e., $D \approx 1.485$). Notice, by comparing Figs. 1 and 2, how the same multifractal measure dx now gets transformed into a distinct projection set dy, whose overall features and textures are, however, similar to those observed in Fig. 1.

As a way of further comparison, Fig. 3 includes a statistical-multifractal analysis of the "signals" in Figs. 1 and 2, that is, the linear and nonlinear counterparts of the notions herein. In addition to the projections themselves (plotted left to right rather than bottom to top), the figures also include the records' autocorrelation functions (with the $\pm e^{-1}$ levels highlighted), their power spectra (plotted as it is customary in a log–log scale) and their multifractal spectra (i.e., their so-called "f vs. α" curves; see Puente and Obregón 1999).

Notice that, although the locations of the main peaks vary, both data sets indeed share a similar degree of complexity, as indicated by similar decay in autocorrelation functions, power-law scaling in their power spectra ($S(\omega) \sim \omega^{\beta}$), and multifractal properties (as reflected by the similar inverted parabolas in their multifractal spectra). More specifically, both signals do share similar statistical-multifractal characteristics, as follows. They have, for the linear and nonlinear cases, respectively, (a) fractal dimensions for the signals D_{dy} of 1.43 and 1.37 (not the dimension of their defining attractors G), (b) correlation scales τ_e (defined when correlation reaches e^{-1}) of 101 and 80 lags, (c) spectral exponents β of −1.21 and −1.08, and (d) entropy dimensions D_1 (the shown intersection between

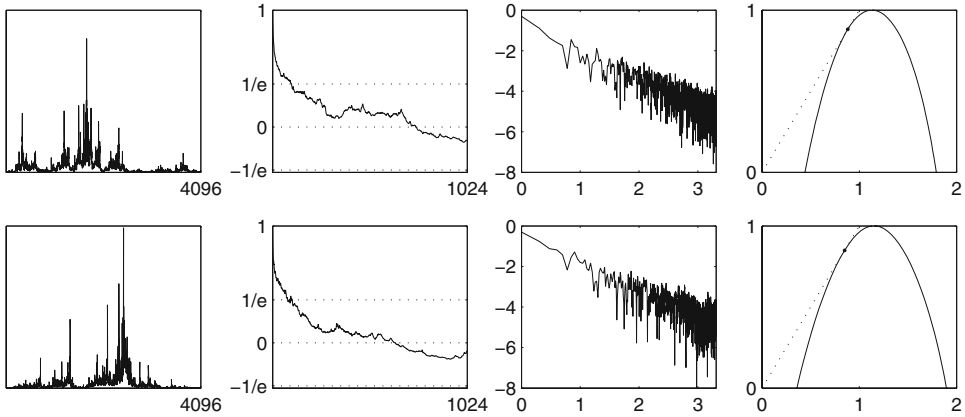

Fig. 3 Statistical and multifractal analyses of *dy* measures corresponding to the linear (*top*) and nonlinear (*bottom*) map cases of Figs. 1 and 2. From left to right: projection time series made of 4,096 values, autocorrelation function computed up to 1,024 lags, power spectrum shown in log–log scale, and multifractal spectrum "f (*vertical*) versus α (*horizontal*)"

the multifractal spectrum and the $f = \alpha$ line) of 0.88 and 0.85.

Overall, these features and characteristics (for both the linear and the nonlinear cases) turn out to be similar to those found in practical environmental applications and beyond (e.g., Puente et al. 1999; Puente 2004). As an example of this fact, Fig. 4 presents a statistical-multifractal analysis for a rainfall storm event measured in Boston (and made of 2,048 values), for which chaotic behavior was identified (Rodríguez-Iturbe et al. 1989). Such a pattern, shown normalized so that its area equals one unit as in the previous projections, yields decay in the autocorrelation function, power-law scaling in the power spectrum, and multifractal properties, which gives $\tau_e = 48$ lags (or approximately 96 for a series having 4,096 values as in Fig. 3), $\beta = -1.74$ and $D_1 = 0.96$. These overall features and characteristics are certainly comparable (although not identical) to those shown in Fig. 3.

From this and other examples (e.g., Obregón et al. 2002a, b; Puente and Sivakumar 2003), it may thus be construed that the enhanced nonlinear fractal-multifractal framework is worthy of further investigation as a candidate to model environmental data sets. In light of this, an initial exploration of the vast array of (deterministic) sets that may be generated via this nonlinear geometric setting is presented next.

4 Sample patterns via the nonlinear fractal–multifractal approach

As analytical derivations of the derived measures and their implied statistical-multifractal properties are extremely difficult, even for the linear case (Puente 1992), the results herein correspond to numerical calculations aimed at identifying the effects of varying some of the parameters of the geometric representation. As varying just a single parameter changes the fractal attractor globally, the exploration herein will also serve as a way to build intuition on the derived patterns that may be generated.

Figure 5 presents a sensitivity analysis around the pattern generated via the linear fractal–multifractal approach shown in Fig. 1 (now portrayed on the top of Fig. 5), by adding the aforementioned cosine perturbation, varying the amplitude A from 0 (i.e., the linear case) to 0.5 in increments of 0.125, while having the frequency parameter fixed at $\omega = 2$. For improved readability, the graphs here (and in the rest of the paper) are not labeled in their axes, but it should be noted that all of them integrate to one. As may be observed, the main chunks as well as the major peaks of these sets, all of which may very well represent reasonable variations of a given environmental phenomenon (e.g., rainfall), travel to the right as A is increased, while leaving close-to-zero values, on the right hand side of the domain, mostly unchanged. As reported in the caption, although

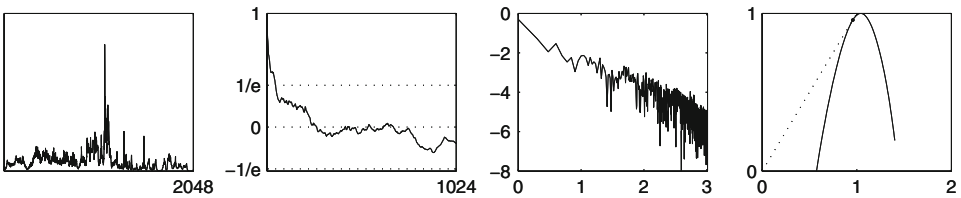

Fig. 4 Statistical and multifractal analyses of a normalized storm data set gathered in Boston. From left to right: time series made of 2,048 values (with the last 58 points set to 0), autocorrelation function computed up to 1,024 lags, power spectrum shown in log–log scale, and multifractal spectrum "f (*vertical*) versus α (*horizontal*)"

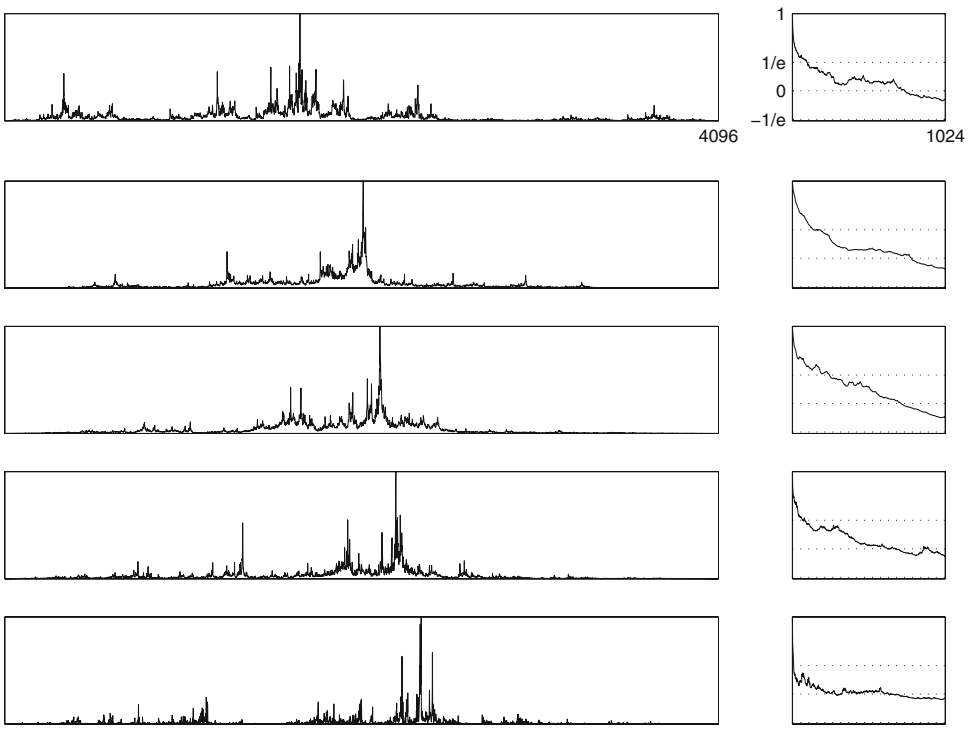

Fig. 5 Sensitivity of derived measure dy to variations in perturbation amplitudes A for a fixed frequency ω. Interpolating points: {(0, 0), (1/2, −0.35), (1, −0.2)}, vertical scalings: $d_1 = -0.8$, $d_2 = -0.6$, parent multifractal parameter: $p = 0.3$, nonlinear perturbation: $g(y) = A \cdot \cos(\omega \cdot y)$, $A = 0$ (*top*) to $A = 0.5$ (*bottom*) in increments of 0.125, $\omega = 1$. Key statistics (*top* to *bottom*): $D = 1.49, 1.56, 1.55, 1.47, 1.30$, $D_{dy} = 1.35, 1.28, 1.30, 1.28, 1.29$, $\tau_e = 101, 146, 250, 74, 10$, $\beta = -1.21, -1.55, -1.45, -1.12, -0.98$, $D_1 = 0.88, 0.89, 0.90, 0.87, 0.74$

these patterns share a similar fractal dimension D_{dy} close to the average value of 1.30, they do not exhibit a monotonic behavior in their other main statistical-multifractal qualifiers. For instance, there are up and down variations in: (a) the fractal dimensions of their underlying attractors D, (b) their correlation scales τ_e, (c) the negative of the spectral exponents β, and (d) their entropy dimensions D_1 (even if only slightly for the first four sets).

It is worth noticing that the last set, corresponding to the lowest attractor dimension D, exhibits more areas of inactivity as compared to the other sets. This happens because such an attractor is less capable than the others of filtering the intermittencies and overall complexity of the parent multifractal measure dx. Due to this fact, the autocorrelation function for such a case decays very fast to 0, the spectral exponent yields a case close to "1/f" noise, and the entropy dimension is low, indicating a high degree of disorganization.

Figure 6 shows a similar sensitivity analysis to the one just mentioned, but varying the frequency parameter ω on the cosine perturbation, while leaving the amplitude fixed at $A = 0.5$. The sets shown correspond to equal increments of ω values ranging from 0.5 (top) to 2.5 (bottom), and, hence, the second pattern from the top corresponds to the one already presented in Fig. 2. Contrary to the previous sensitivity analysis, the signals here maintain the locations of their main chunks and major peaks when the frequency parameter is varied. Also, some noticeable trends may be discerned regarding their statistical-multifractal attributes, as detailed in the caption of the figure: (a) the fractal dimensions of the attractors D and signals D_{dy} decrease, (b) their correlation scales τ_e tend to decrease, and (c) the entropy dimensions D_1 also decrease.

Although results regarding the power spectral exponent β are not equally conclusive for these cases, what was said of the last pattern in Fig. 5 may also be said of the last two sets in Fig. 6. As the fractal dimensions of their underlying attractors D are significantly lower than the other signals, such attractors reflect, to a larger degree than those with higher dimensions, the intricacies of the highly irregular parent multifractal measure dx. Overall, and for the particular set of parameters used, an increasingly oscillating perturbation (i.e., as ω increases) has the ultimate effect of smoothing the attractor G, leading to more complex (i.e., lower τ_e and D_1) derived patterns. However, care must be exercised, as shall be noted later, for an increase in frequency does not necessarily imply a smoothing of an attractor for other sets of parameters.

As a means of continuing the exploration, Fig. 7 presents other patterns obtained via a sensitivity analysis of another more erratic set as computed via the linear fractal-multifractal methodology (Puente 2004, Fig. 7). Specifically, all patterns correspond to the interpolating points {(0, 0), (0.3, 1), (1, 0)}, vertical scalings $d_1 = 0.4$, $d_2 = -0.5$, a parent multifractal parameter $p = 0.4$, a projection angle $\theta = -20°$, when varying the cosine amplitude A from 0 (i.e., the linear case) to 1 in increments of 0.25, while having the frequency set at $\omega = 0.05$. Given that the fractal dimensions of the attractors are lower than 1.2, all patterns exhibit an intense level of activity reminiscent of

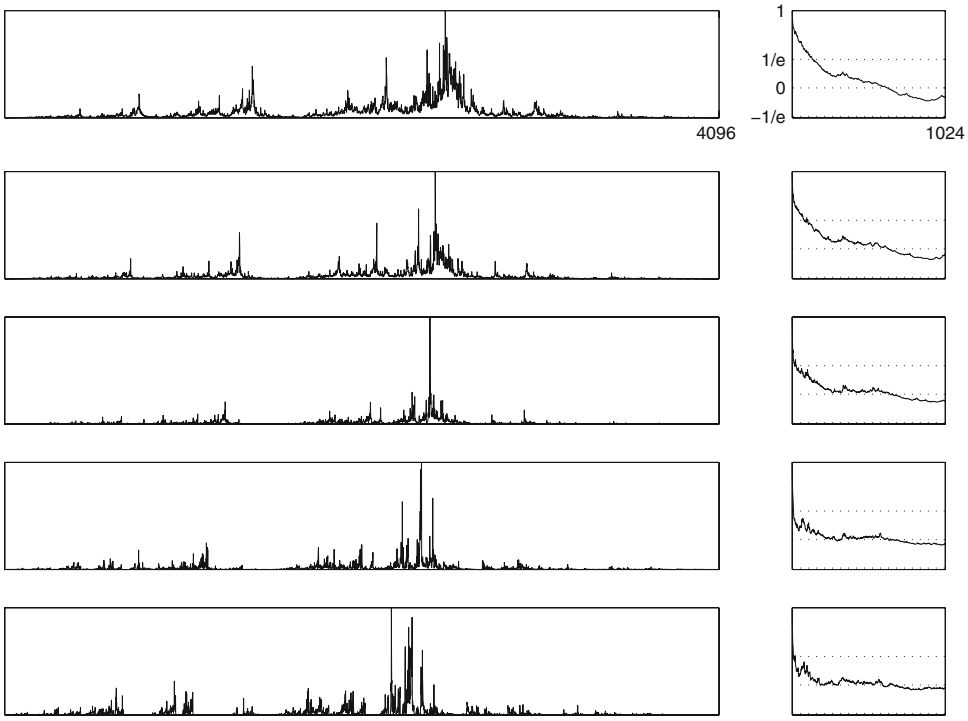

Fig. 6 Sensitivity of derived measure dy to variations in perturbation frequencies ω for a fixed amplitude A. Interpolating points: {(0, 0), (1/2, −0.35), (1, −0.2)}, vertical scalings: $d_1 = -0.8$, $d_2 = -0.6$, parent multifractal parameter: $p = 0.3$, nonlinear perturbation: $g(y) = A \cdot \cos(\omega \cdot y)$, $A = 0.5$, $\omega = 0.5$ (*top*) to $\omega = 2.5$ (*bottom*) in increments of 0.5. Key statistics (*top* to *bottom*): $D = 1.49, 1.47, 1.41, 1.30, 1.19$, $D_{dy} = 1.37, 1.31, 1.29, 1.29, 1.31$, $\tau_e = 137, 80, 19, 10, 10$, $\beta = -1.21, -1.08, -0.99, -0.98, -1.00$, $D_1 = 0.87, 0.85, 0.81, 0.74, 0.68$

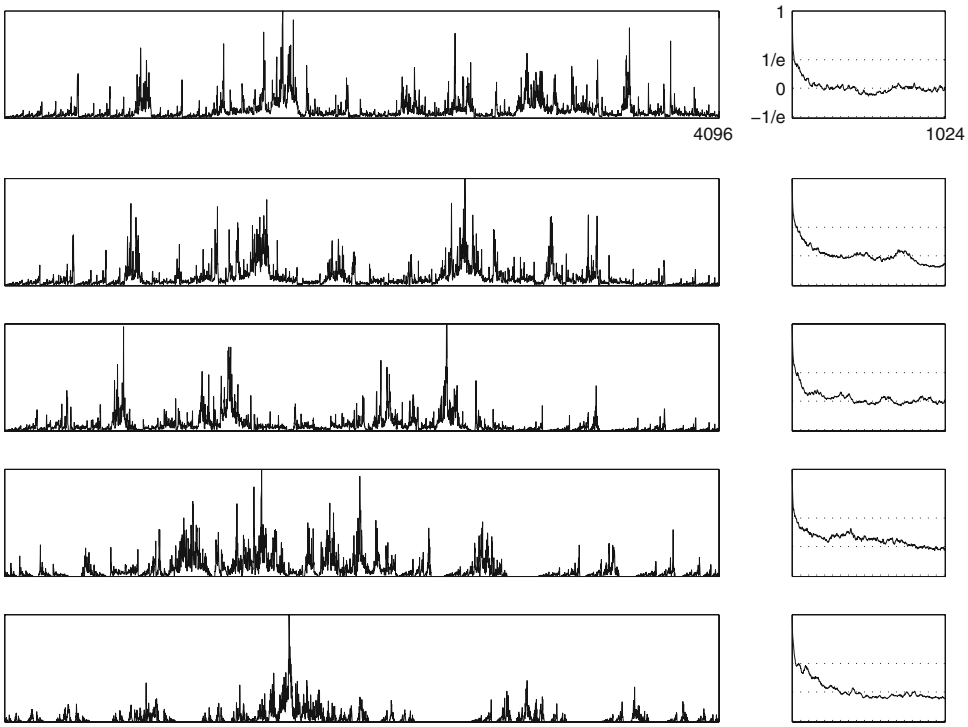

Fig. 7 Sensitivity of derived measure dy to variations in perturbation amplitudes A for a fixed frequency ω. Interpolating points: {(0, 0), (0.3, 1), (1, 0)}, vertical scalings: $d_1 = 0.4$, $d_2 = -0.5$, parent multifractal parameter: $p = 0.4$, projection angle: $\theta = -20°$, nonlinear perturbation: $g(y) = A \cdot \cos(\omega \cdot y)$, $A = 0$ (*top*) to $A = 1.0$ (*bottom*) in increments of 0.25, $\omega = 0.05$. Key statistics (*top* to *bottom*): $D = 1.20, 1.20, 1.20, 1.15, 1.12$, $D_{dy} = 1.42, 1.42, 1.40, 1.42, 1.38$, $\tau_e = 14, 27, 25, 25, 25$, $\beta = -1.14, -1.08, -1.13, -1.07, -1.11$, $D_1 = 0.91, 0.90, 0.88, 0.88, 0.76$

environmental signals that exhibit periodicities. As already found in Fig. 5, when the amplitude increases significantly, the resulting signal contains periods of no activity and has an increasing complexity.

Notice how these deterministic "simulations," that may perhaps be interpreted as realizations of a stochastic process, may indeed be used to describe, in their entirety, the otherwise apparent randomness found in nature. This is certainly a notable feature of these ideas that cannot be easily matched by stochastic approaches, which by definition yield realizations that only match some of the statistical-multifractal properties of the records. Observe

that although the patterns in Fig. 7 show very similar statistical-multifractal characteristics, they are quite different from one another. This fact implies that such attributes by themselves can not characterize the variety of patterns herein, and serves as a further reminder that they can not be used for natural data sets either.

Figure 8 further explores the parameter space of the nonlinear projections via a sensitivity analysis on the frequency ω, as in Fig. 6. Specifically, the patterns correspond to the interpolating points {(0, 0), (1/2, 5), (1, 4)}, vertical scalings $d_1 = 0.9$, $d_2 = -0.4$, a parent multifractal parameter of $p = 0.6$, a projection angle $\theta = 10°$, when varying the cosine frequency ω from 0.5 to 2.5 in increments of 0.5, while having the amplitude fixed at $A = 0.5$. As may be discerned, none of the patterns shown corresponds to a linear fractal-multifractal case. While the top pattern is reminiscent of other already found in this brief exploration, the others show another host of plausible natural sets having realistic statistical-multifractal qualifiers. Notice that, unlike the results presented in Fig. 6, an increase in the parameter ω does not lead to a smoothing of an attractor. In conclusion, the sensitivity of our procedure on the parameter ω is quite complex and not intuitive, as the interplay between the iterations and the perturbation is not trivial.

If the patterns shown were interpreted as hydrographs, observe how the second one from the top would correspond to perhaps a single event coming from a sustained rain. Such a pattern is also reminiscent of the width-function of natural river networks (i.e., the number of links as a function of the distance to the basin's outlet, Puente and Sivakumar 2003).

Figure 9 further illustrates that other plausible width-functions may be obtained from appropriate variations in the amplitude parameters of the nonlinear perturbations of a linear (bottom) fractal-multifractal projection (Puente 2004; Fig. 6). As may be seen, the statistics of these patterns (except for the power spectral exponent) are quite similar, yet the actual distributions exhibit distinct shapes that may reflect alternative inner structures of natural river networks. A relevant research question that these sets inspire is to study how the parameters of the width function may change in nature as a response to erosion mechanisms. Based on our results, this may perhaps be addressed via variations in the parameters of the (nonlinear) projections herein.

As the choice of the bounded nonlinear perturbation is clearly arbitrary, Fig. 10 shows an example of what can be obtained by varying the functional shape of the nonlinear perturbation. In this example, a sigmoid function $g(y) = A \cdot (1 + \exp(-\omega \cdot y))^{-1}$ is used. As done before, a sensitivity analysis is presented based on the linear case used in Figure 1, varying the amplitude A from 0 (i.e., the linear case) to 0.5 in increments of 0.125, while keeping the "frequency" at $\omega = 2$. Notice that, for the set of parameters used, the choice of this perturbation leads to fractal attractors of increasing dimensions, which leads to increasing filtering of the parent multifractal, as reflected

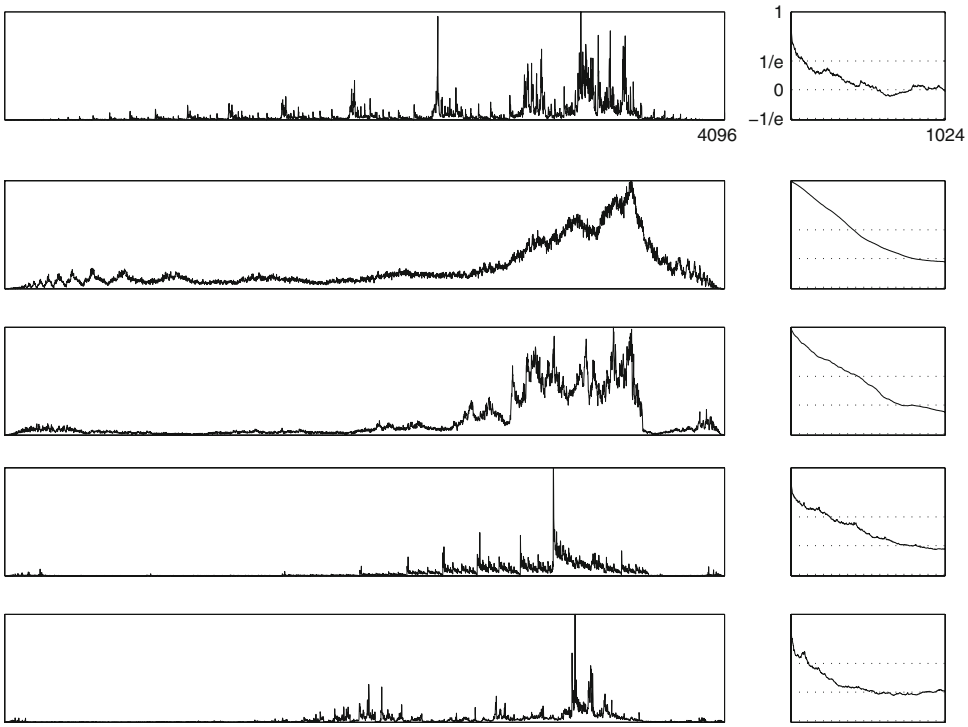

Fig. 8 Sensitivity of derived measure dy to variations in perturbation frequencies ω for a fixed amplitude A. Interpolating points: {(0, 0), (1/2, 5), (1, 4)}, vertical scalings: $d_1 = 0.9$, $d_2 = -0.4$, parent multifractal parameter: $p = 0.6$, projection angle: $\theta = 10°$, nonlinear perturbation: $g(y) = A \cdot \cos(\omega \cdot y)$, $A = 0.5$, $\omega = 0.5$ (*top*) to $\omega = 2.5$ (*bottom*) in increments of 0.5. Key statistics (*top* to *bottom*): $D = 1.19$, 1.50, 1.53, 1.13, 1.54, $D_{dy} = 1.37$, 1.44, 1.41, 1.29, 1.30, $\tau_e = 85$, 417, 448, 262, 120, $\beta = -1.11$, -1.00, -1.58, -1.27, -1.00, $D_1 = 0.81$, 0.94, 0.91, 0.86, 0.85

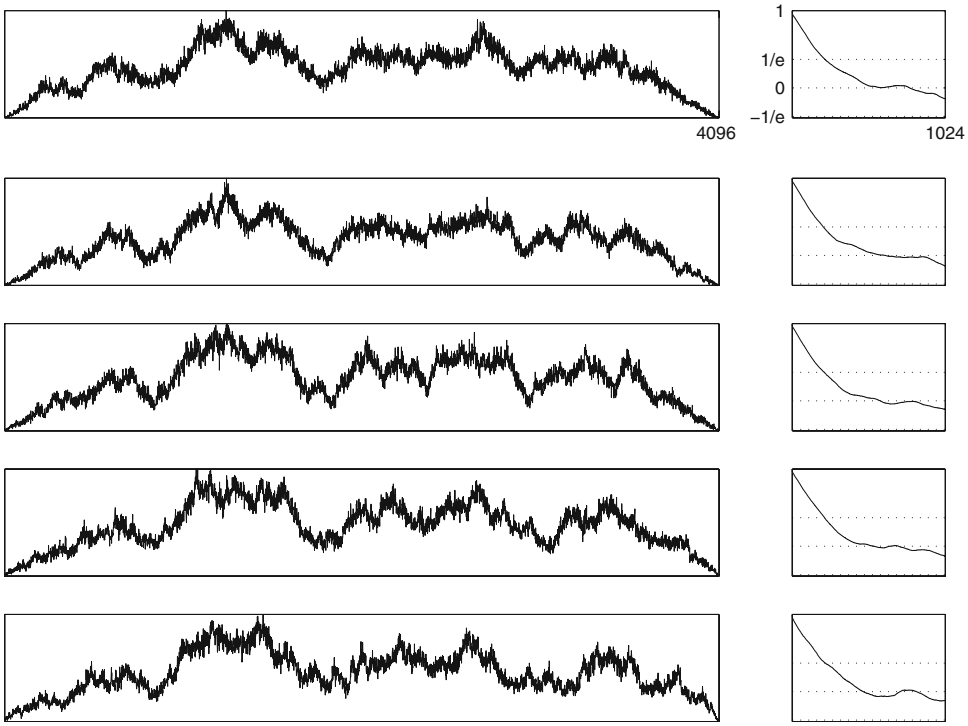

Fig. 9 Sensitivity of derived measure *dy* to variations in perturbation amplitudes A for a fixed frequency ω. Interpolating points: {(0, 0), (1/2, 1), (1, 0)}, vertical scalings: $d_1 = 0.7$, $d_2 = -0.7$, parent multifractal parameter: $p = 0.5$, projection angle: $\theta = 20°$, nonlinear perturbation: $g(y) = A \cdot \cos(\omega \cdot y)$, $A = -0.5$ (*top*) to $A = 0$ (*bottom*) in increments of 0.125, $\omega = 0.5$. Key statistics (*top* to *bottom*): $D = 1.57$, 1.56, 1.55, 1.55, 1.55, $D_{dy} = 1.49$, 1.49, 1.49, 1.49, 1.50, $\tau_e = 222$, 210, 216, 218, 224, $\beta = -0.66$, -0.66, -0.72, -0.75, -0.80, $D_1 = 0.99$, 0.99, 0.99, 0.99, 0.99

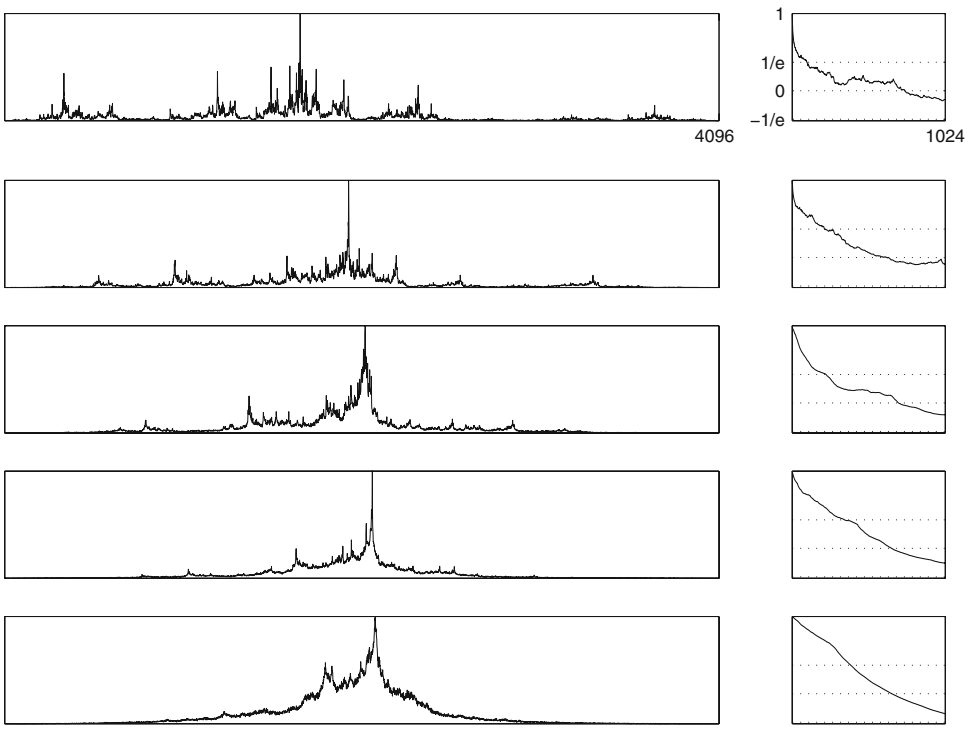

Fig. 10 Sensitivity of derived measure *dy* to variations in perturbation amplitudes A for a fixed frequency ω. Interpolating points: {(0, 0), (1/2, -0.35), (1, -0.2)}, vertical scalings: $d_1 = -0.8$, $d_2 = -0.6$, parent multifractal parameter: $p = 0.3$, projection angle: $\theta = 0°$, nonlinear perturbation: $g(y) = A \cdot (1 + e^{-\omega \cdot y})^{-1}$, $A = 0$ (*top*) to $A = 0.5$ (*bottom*) in increments of 0.125, $\omega = 2$. Key statistics (*top* to *bottom*): $D = 1.50$, 1.57, 1.62, 1.67, 1.72, $D_{dy} = 1.35$, 1.30, 1.27, 1.22, 1.26, $\tau_e = 101$, 218, 228, 353, 394, $\beta = -1.21$, -1.51, -1.57, -1.66, -1.43, $D_1 = 0.88$, 0.91, 0.88, 0.89, 0.89

by an increasing correlation scale. Clearly, this graph represents just an example of the manifold possibilities of extensions that can be envisaged when looking for geometric representations of natural patterns.

In order to further appreciate the nature of the results presented herein, Fig. 11 shows a case when a uniformly random distribution, with varying amplitude, is used instead of a nonlinear perturbation. This is included as one might think that adding $A \cdot \cos(\omega \cdot y)$ to the linear maps may be equivalent to adding just a random signal, especially for high frequencies. As may be seen, however, increasing the amplitude of an added noise tends unequivocally to a local

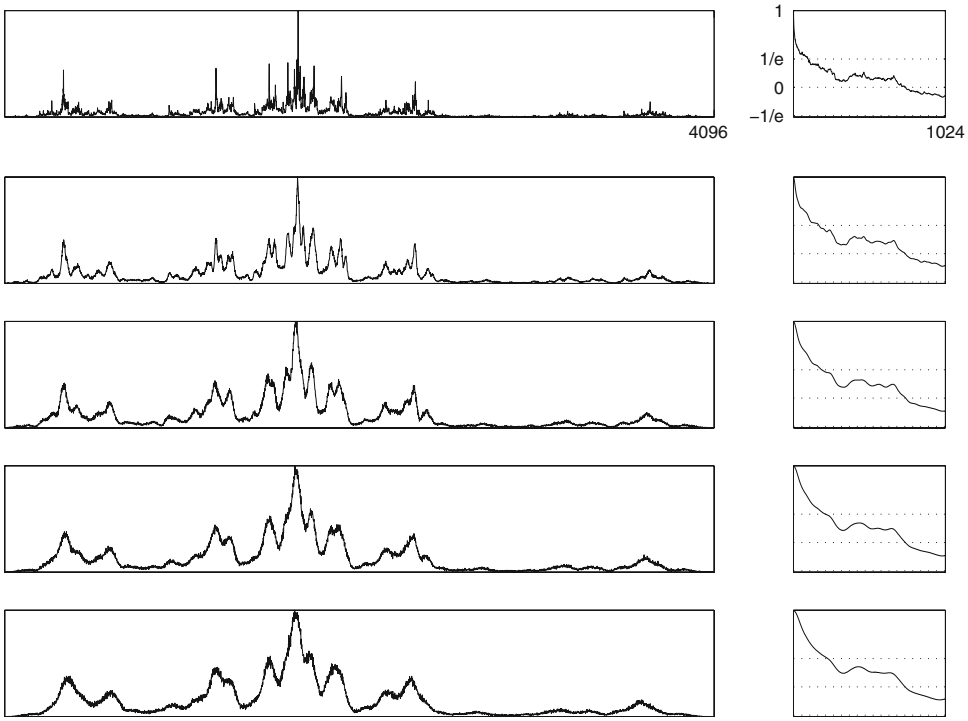

Fig. 11 Sensitivity of derived measure *dy* to variations in perturbation amplitudes A of a uniform noise perturbation. Interpolating points: {(0, 0), (1/2, −0.35), (1, −0.2)}, vertical scalings: $d_1 = -0.8$, $d_2 = -0.6$, parent multifractal parameter: $p = 0.3$, projection angle: $\theta = 0°$, noise characteristics: $A = 0$ (*top*) to $A = 0.005$ (*bottom*) in increments of 0.00125. Key statistics (*top* to *bottom*): $D = 1.50, 1.50, 1.51, 1.52, 1.53$, $D_{dy} = 1.35, 1.38, 1.40, 1.39, 1.40$, $\tau_e = 101, 174, 192, 219, 234$, $\beta = -1.21, -1.60, -1.15, -0.97, -0.82$, $D_1 = 0.88, 0.90, 0.91, 0.92, 0.92$

smoothing of the derived measure (i.e., as in Fig. 1), and such extensions are not that interesting.

Finally, it is relevant to mention that drastically increasing the amplitude of an added perturbation (cosine or sigmoid or even random) yields derived measures *dy* that converge towards a Gaussian distribution, even when the underlying attractors do not fill up space. This result turns out to generalize the already nontrivial roads to Gaussianity found via fractal interpolating functions and the linear case (Puente et al. 1996). Details of these extended results shall be reported elsewhere.

5 Summary

It has been illustrated that extensions of the fractal–multifractal approach, obtained by adding nonlinear and bounded perturbations to the linear equations to be iterated, yield fractal attractors not shaped as continuous fractal interpolating functions that, nonetheless, result in a multitude of derived measures that resemble patterns found in environmental applications. Such patterns are relevant in practice as they: (a) vastly extend the already numerous scenarios defined via the original linear framework, (b) may be easily calculated at any resolution, and (c) result in substantial compression ratios that, given the small number of parameters, easily exceed ratios of 100:1.

In regards to the sensitivity cases shown herein, and many others not reported, the following general trends may be established: (a) the derived projection patterns *dy* depend, in a rather nontrivial way, on the nature of the nonlinear perturbation added, whose most general functional form may be defined as $g(y) = A \cdot h(\omega \cdot y)$, for a suitable bounded function h, (b) "small" variations in the amplitude A (at small constant ω) yield more stable sensitivity scenarios than "small" variations in the "frequency" ω for fixed amplitudes, (c) the patterns obtained by adding the nonlinear perturbations are not equivalent to those obtained by adding a white-noise, as may perhaps be thought of, for an increase in the amplitude of the noise progressively smooths out a given signal, and (d) there are many combinations of the nonlinear parameters that yield a Gaussian distribution as the derived pattern, *dy*, even though the parameters of the linear maps do not imply a space-filling attractor, as previously required on the linear fractal–multifractal approach.

This work has shown that nonlinear extensions of the fractal–multifractal approach represent a viable alternative to existing stochastic methods for the modeling of environmental information. This is so because the geometric approach may (in principle) handle data sets in their entirety, and not simply as plausible realizations that are typically difficult to condition. These results therefore hint at the possibility of hidden (nontrivial) determinism within natural complexity via the projection ideas.

In a practical setting, the effective use of these ideas depends (of course) on the resolution of a required inverse problem for a given pattern. This problem, however, and as hinted by the nature of the results herein, and those found for the original linear case, is a rather challenging one. This

is due to the fact that similar patterns may be obtained from different parameter values (i.e., equifinality) and because the lack of analytical expressions implies an optimization problem that can only be solved numerically. We are working on this problem via the use of neuro-fuzzy neural networks and swarm intelligence computation, and results shall be reported elsewhere.

Pending the resolution of such a problem, we envision however that these notions (and other procedures aiming to capture mathematical morphology explicitly) may result in a more complete understanding of complex environmental systems and the dynamics of the patterns they produce. This is particularly so, as the evolution of records may perhaps be discerned in the compressed parameter space of subsequent sets, without the need of resorting to difficult-to-solve (stochastic) differential equations whose structure and initial conditions may not be easily determined (Puente et al. 2001a, b). It is our hope that these geometry-based ideas aimed at capturing what we observe, that is, the data, would make further inroads in environmental research.

Acknowledgments This work was supported in part by the Director, Office of Science, of the US Department of Energy under Contract No. DE-AC02-05CH11231.

References

Barnsley MF (1986) Fractal functions and interpolation. Constr Approx 2:303–329

Barnsley MF (1988) Fractals everywhere. Academic Press, New York

Box G, Jenkins GM, Reinsel G (1994) Time series analysis: forecasting and control. Prentice-Hall, New York

Lorenz EN (1963) Deterministic nonperiodic flow. J Atmos Sci 20:130–141

Mandelbrot BB (1983) The fractal geometry of nature. Freeman, New York

Mandelbrot BB (1989) Multifractal measures especially for the geophysicist. In: Scholz CH, Mandelbrot MM (eds) Fractals in geophysics. Birkhauser Verlag, Basel, pp 1–42

Meneveau C, Sreenivasan KR (1987) Simple multifractal cascade model for fully developed turbulence. Phys Rev Lett 59:1424–1427

Obregón N, Puente CE, Sivakumar B (2002a) Modeling high resolution rain rates via a deterministic fractal–multifractal approach. Fractals 10(3):387–394

Obregón N, Sivakumar B, Puente CE (2002b) A deterministic geometric representation of temporal rainfall. Sensitivity analysis for a storm in Boston. J Hydrol 269(3–4):224–235

Puente CE (1992) Multinomial multifractals, fractal interpolators, and the Gaussian distribution. Phys Lett A 161:441–447

Puente CE (1994) Deterministic fractal geometry and probability. Int J Bifurcat Chaos 4(6):1613–1629

Puente CE (1996) A new approach to hydrologic modeling: Derived distributions revisited. J Hydrol 187:65–80

Puente CE (2004) A universe projections: may Plato be right? Chaos Solitons Fractals 19(2):241–253

Puente CE, Obregón N (1996) A deterministic geometric representation of temporal rainfall. Results for a storm in Boston. Water Resour Res 32(9):2825–2839

Puente CE, Obregón N (1999) A geometric Platonic approach to multifractality and turbulence. Fractals 7(4):403–420

Puente CE, Sivakumar B (2003) A deterministic width function model. Nonlinear Process Geophys 10:525–529

Puente CE, Sivakumar B (2007) Modeling hydrologic complexity: a case for geometric determinism. Hydrol Earth Syst Sci 11:721–724

Puente CE, López MM, Pinzón JE, Angulo JM (1996) The Gaussian distribution revisited. Adv Appl Prob 28(2):500–524

Puente CE, Obregón N, Robayo O, Juliao MG, Simsek D (1999) Projections of fractal functions: a new vision to nature's complexity. Fractals 7(4):387–401

Puente CE, Robayo O, Díaz MC, Sivakumar B (2001a) A fractal–multifractal approach to groundwater contamination. 1. Modeling conservative tracers at the Borden site. Stoch Environ Res Risk Assess 15(5):357–371

Puente CE, Robayo O, Sivakumar B (2001b) A fractal–multifractal approach to groundwater contamination. 2. Predicting conservative tracers at the Borden site. Stoch Environ Res Risk Assess 15(5):372–383

Rodríguez-Iturbe I, De Power FB, Sharifi MB, Georgakakos KP (1989) Chaos in rainfall. Water Resour Res 25(7):1667–1675

Yaglom AM (1987) Correlation theory of stationary and related random functions. Springer, New York